

# Cyclical period changes in the dwarf novae V2051 Oph and V4140 Sgr <sup>★</sup>

R. Baptista <sup>1</sup>, B. W. Borges <sup>1</sup>, H. E. Bond <sup>2</sup>,  
F. Jablonski <sup>3</sup>, J. E. Steiner <sup>4</sup> and A. D. Grauer <sup>5</sup>

<sup>1</sup> *Departamento de Física, UFSC, Campus Trindade, 88040-900, Florianópolis, Brazil*

<sup>2</sup> *Space Telescope Science Institute, 3700 San Martin Drive, Baltimore, MD 21218, USA*

<sup>3</sup> *Divisão de Astrofísica, Instituto Nacional de Pesquisas Espaciais, S. J. dos Campos, Brazil*

<sup>4</sup> *Departamento de Astronomia - IAG, Universidade de São Paulo, São Paulo, Brazil*

<sup>5</sup> *Dept. of Physics & Astronomy, University of Arkansas, Little Rock, AR 72204, USA*

Accepted 2003 July 15. Received 2003 July 7; in original form 2003 April 10

## ABSTRACT

We report the identification of cyclical changes in the orbital period of the eclipsing dwarf novae V2051 Ophiuchi and V4140 Sagittarii. We used sets of white dwarf mid-eclipse timings to construct observed-minus-calculated diagrams covering, respectively, 25 and 16 years of observations. The V2051 Oph data present cyclical variations that can be fitted by a linear plus sinusoidal function with period  $22 \pm 2$  yr and amplitude  $17 \pm 3$  s. The statistical significance of this period by an F-test is larger than 99.9 per cent. The V4140 Sgr data present cyclical variations of similar amplitude and period  $6.9 \pm 0.3$  yr which are statistically significant at the 99.7 per cent level. We derive upper limits for secular period changes of  $|\dot{P}| < 3 \times 10^{-12}$  and  $|\dot{P}| < 1.8 \times 10^{-11}$ , respectively for V2051 Oph and V4140 Sgr.

We combined our results with those in the literature to construct a diagram of the amplitude versus period of the modulation for a sample of 11 eclipsing cataclysmic variables (CVs). If the cyclical period changes are the consequence of a solar-type magnetic activity cycle in the secondary star, then magnetic activity is a widespread phenomenon in CVs, being equally common among long- and short-period systems. This gives independent evidence that the magnetic field (and activity) of the secondary stars of CVs do not disappear when they become fully convective. We also find that the fractional cycle period changes of the short-period CVs are systematically smaller than those of the long-period CVs.

**Key words:** accretion, accretion discs – stars: dwarf novae – stars: evolution – binaries: eclipsing – stars: individual: V2051 Oph, V4140 Sgr.

## 1 INTRODUCTION

Cataclysmic variables (CVs) are mass-transferring binary systems containing a white dwarf accretor (the primary) and a late-type donor star (the secondary). If the white dwarf is not strongly magnetized ( $B \lesssim 10^6$  Gauss) the transferred matter forms an accretion disc with a bright spot at the position where the stream of matter hits the outer edge of the disc.

In most CVs the donor star has lower mass than the accreting star. Since conservative mass transfer in such sit-

uations would lead to an increase in the orbital separation (and therefore the cessation of mass transfer via Roche lobe overflow), the existence of CVs as mass-transfer binaries implies that they must continuously lose angular momentum in order to sustain the mass transfer process. As a consequence, the binary should evolve slowly towards shorter orbital periods (on time scales of  $10^8 - 10^9$  yr). Possible mechanisms suggested for driving the continuous angular momentum loss are magnetic braking via the secondary star's wind (for  $P_{orb} > 3$  hr) and gravitational radiation (for  $P_{orb} < 3$  hr) (King 1988). At very short periods, when the secondary star becomes fully degenerate ( $M_2 \lesssim 0.08 M_\odot$ ), mass loss leads to an expansion of this star and reverses the secular trend, resulting thereafter in an increasing orbital period. However, the predicted mass transfer rate after this period

<sup>★</sup> email: bap@astro.ufsc.br (RB); bernardo@astro.ufsc.br (BWB); bond@stsci.edu (HEB); chico@das.inpe.br (FJJ); steiner@astro.iag.usp.br (JES); adgrauer@ualr.edu (ADG)

minimum is low ( $\dot{M}_2 \simeq 10^{-12} M_\odot \text{ yr}^{-1}$ ) and few CVs are expected to be observed in such evolutionary stage (Warner 1995).

CVs show a bi-modal distribution of orbital periods, with systems clustering at periods of 1.5 – 2 hr or 3 – 5 hr, and a remarkable dearth of systems with periods between 2 – 3 hr. This *period gap* is explained in terms of the secular evolution of the binary by the interrupted braking model (e.g., Hameury, King & Lasota 1991): At periods above the gap, relatively rapid loss of angular momentum (via magnetic wind) drives the donor star out of thermal equilibrium and makes it oversized for its mass compared with its main sequence radius. When the period reaches 3 hr, the angular momentum losses are sharply reduced, possibly in consequence of a reduced number of open field lines as the star becomes fully convective. The star then shrinks back to its main sequence radius and detaches from the Roche lobe, halting mass transfer. Angular momentum losses continue, but on a longer time scale set by gravitational radiation, and reduces the binary separation until at  $P_{orb} \simeq 2$  hr the Roche lobe eventually closes down on the star and mass transfer resumes at lower  $\dot{M}$ .

The secular evolution of the binary can in principle be detected by measuring the changes in the orbital period of eclipsing CVs. Eclipses provide a fiducial mark in time and can usually be used to determine the orbital period (and its derivative) with high precision. However, attempts to measure the long-term orbital period decrease in CVs have been disappointing: none of the studied stars show a positive detection of an orbital period decrease (e.g., Beuermann & Pakull 1984). Instead, essentially all of the well observed eclipsing CVs<sup>†</sup> show cyclical period changes (e.g., Bond & Freeth 1988; Warner 1988; Robinson, Shetrone & Africano 1991; Baptista, Jablonski & Steiner 1992; Echevarria & Alvarez 1993; Wolf et al. 1993; Baptista et al. 1995; Baptista, Catalán & Costa 2000; Baptista et al. 2002).

The most promising explanation of this effect seems to be the existence of a solar-type (quasi- and/or multi-periodic) magnetic activity cycle in the secondary star modulating the radius of its Roche lobe and, via gravitational coupling, the orbital period on time scales of the order of a decade (Applegate 1992; Richman, Applegate & Patterson 1994). The relatively large amplitude of these cyclical period changes probably contributes to mask the low amplitude, secular period decrease.

In this paper we report the results of an investigation of orbital period changes in the short-period CVs V2051 Oph and V4140 Sgr. The revised (O–C) diagrams show cyclical period changes similar to those observed in many other well studied eclipsing CVs. The observations and data analysis are presented in section 2 and the results are discussed and summarized in section 3.

<sup>†</sup> i.e., those with well-sampled observed-minus-calculated (O–C) eclipse timings diagram covering more than a decade of observations.

## 2 OBSERVATIONS AND DATA ANALYSIS

### 2.1 V2051 Oph

Our observations of V2051 Oph date back to the night in 1977 when the eclipses were first discovered by Bond (1977) with one of the 0.9-m telescopes at Kitt Peak National Observatory (KPNO) (Actually, the very first eclipse was seen visually by Bond when V2051 Oph disappeared while he was identifying the star at the eyepiece!). Between 1977 and 1979, we timed eclipses of V2051 Oph with the 0.9-m telescopes at KPNO, Cerro Tololo Interamerican Observatory (CTIO), and the Louisiana State University (LSU) Observatory. Most of the data comprises observations collected with the 1.6 m telescope at Laboratório Nacional de Astrofísica (LNA) in Brazil from 1981 to 2002. We also observed V2051 Oph with the Hubble Space Telescope (HST) on 1996 January 29.

All the KPNO, CTIO and LSU runs, as well as the LNA observations prior to 1998, were made with photoelectric photometers in a time-series acquisition mode using bi-alkali or GaAs photomultiplier tubes. The data include runs in white light (W) and in the Johnson-Cousins UB–VRI system. The raw data were sky-subtracted. Correction for extinction and transparency variations at the LSU Observatory was done based on simultaneous measurements of a nearby comparison star, using a two-star high-speed photometer (see Grauer & Bond 1981). For the other runs, these effects were corrected either by frequent observations of a close comparison star or by using extinction coefficients calculated from observations of photometric standard stars of Graham (1982) and Landolt (1983). The UB–VRI observations were reduced to the standard system by means of transformation coefficients for each night, derived from observations of blue spectrophotometric standards (Stone & Baldwin 1983) and standard stars of Landolt (1983) and Graham (1982). We used the relations of Lamla (1981) to transform UB–VRI magnitudes to flux units.

The remaining LNA observations (from 1998 onward) were made in the *B*-band with a high-speed CCD photometer. Data reduction for these data sets included bias subtraction, flat-field correction, cosmic rays removal, aperture photometry extraction and absolute flux calibration. Time-series were constructed by computing the magnitude difference between the variable and a reference comparison star.

The HST runs consist of time-resolved spectroscopy of two consecutive eclipses of V2051 Oph collected with the Faint Object Spectrograph (FOS) on 1996 January 29. The reader is referred to Baptista et al. (1998) for a detailed description of the data set and of the reduction procedures.

For the photoelectric observations, the internal clock of the photometers were manually synchronized to UTC time from a WWV radio signal every night to a precision better than 0.5 s. The absolute timing accuracy of the HST/FOS observations is better than 0.25 s. The CCD photometer has a GPS board which sets its internal clock to UTC time to a precision better than 10 ms.

A summary of the observations is given in Table 1. The third column gives the time resolution of the observations in seconds. The fourth column lists the eclipse cycle number. The data comprise 80 eclipse light curves spanning 25 yr of observations. All data sets were obtained while V2051 Oph was in quiescence.

**Table 1.** Journal of the observations of V2051 Oph.

Date (UT)	Passband	$\Delta t$ (s)	Cycles
1977 Apr 12	W	27.7	0
1977 Apr 13	W	12.5	15, 16
1977 Apr 15	W	6.4	47, 48
1977 Jun 22	W	12.1	1 134
1977 Jun 24	W	12.5	1 164, 1 165
1977 Sep 11	W	10.7	2 430
1977 Sep 12	W	10.3	2 446
1978 Apr 16	W	10.7	5 911
1979 Jun 19	W	5.8	12 778, 12 779
1981 Mar 11	W	10	22 887, 22 888
1981 Jun 10	W	10	24 342
1982 May 16	W	10	29 789
1988 May 11	W	25.2	64 820
1988 Jul 14	W	19.3	65 844, 65 845
1989 Apr 11	WUBVRI	3	70 188-70 190
1989 Jun 06	WUBVRI	3	71 082-71 084
1989 Jun 07	WUBVRI	3	71 089
	WUBVRI	3	71 099, 71 100
1989 Jun 08	WUBVRI	3	71 114, 71 115
1989 Aug 04	WUBVRI	10	72 028
1990 Mar 26	WUBVRI	3	75 781
1990 Aug 13	WUBVRI	3	78 034, 78 036
1990 Aug 14	WUBVRI	3	78 050
1990 Aug 15	WUBVRI	3	78 066
1991 Mar 15	W	5	81 451
1991 Mar 17	W	10	81 482
1991 Mar 18	W	5	81 498, 81 499
1991 Sep 04	WUBVRI	3	84 233
1991 Sep 05	WUBVRI	3	84 249
1992 Jul 29	V	30	89 503-89 505
1996 Jan 29	G400H	3.4	109 988
	G160L	3.4	109 989
1996 Jun 15	B	5	112 201
1996 Jun 16	W	5	112 217, 112 218
1996 Jun 17	W	5	112 233
1998 Jul 25	B	5	124 535-124 537
1998 Jul 26	B	5	124 551-124 555
1999 Jul 12	B	5	130 174, 130 177
1999 Jul 15	B	5	130 222-130 223
2000 Jul 28	B	5	136 293-136 295
2001 Jun 25	B	5	141 611, 141 612
	B	10	141 613, 141 615
2001 Jun 27	B	10	141 643-141 645
	B	10	141 648
2001 Jun 28	B	15	141 660, 141 661
2002 Aug 04	B	10	148 099, 148 100
2002 Aug 07	B	20	148 147

We assigned cycle zero to our first eclipse. Thus, in our cycle counting scheme the first eclipse in the ephemeris of Bauermann & Pakull (1984) is cycle 12778, while that in the ephemeris of Warner & O’Donoghue (1987) corresponds to cycle 24690. A more complete analysis of the optical data will be presented in a separate paper. Here we will concentrate on the measurement of the mid-eclipse times.

Mid-eclipse times were measured from the mid-ingress and mid-egress times of the white dwarf eclipse using the derivative technique described by Wood, Irwin & Pringle (1985). For a given observational season, all light curves were phase-folded according to a test ephemeris and sorted in phase to produce a combined light curve with increased phase resolution. The combined light curve is smoothed with a median filter and its numerical derivative is calculated. A

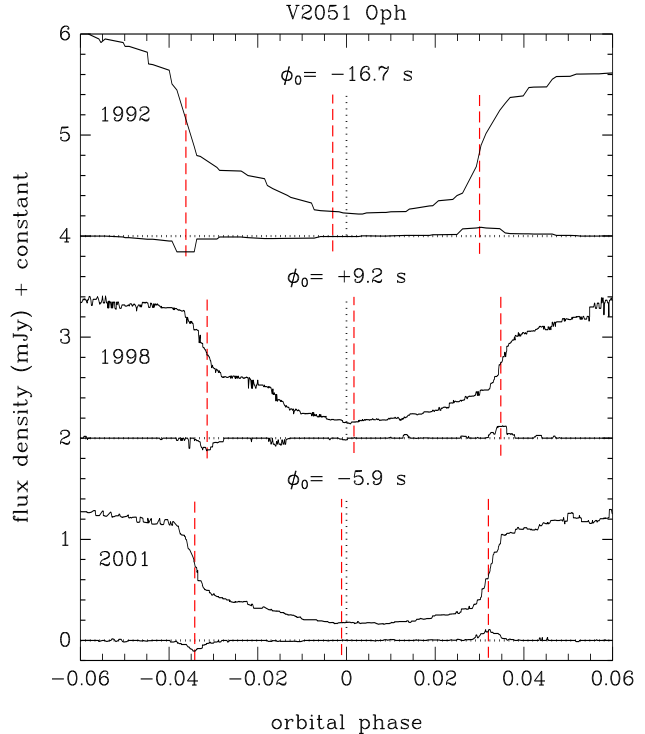


**Figure 1.** Measuring eclipse timings with the derivative technique. The panels show median-filtered average light curves and corresponding median-filtered derivative curves of V2051 Oph for 1992 (top), 1998 (middle) and 2001 (bottom). The 1992 and 1998 curves were vertically displaced by, respectively, 2 and 4 mJy for visualization purposes. Horizontal dotted lines indicate the true zero level in each case. Vertical dashed lines mark the phases of minimum/maximum derivative (mid-ingress/egress of the white dwarf) and the mid-eclipse phase,  $\phi_0$ . A vertical dotted line depicts phase zero. The light curves were phase-folded according to the best-fit linear ephemeris of Table 3. The time difference between mid-eclipse and phase zero is indicated in each panel.

median-filtered version of the derivative curve is then analyzed by an algorithm which identifies the points of extrema (the mid-ingress / egress phases of the white dwarf). The mid-eclipse phase,  $\phi_0$ , is the mean of the two measured phases. In all cases the difference between the measured mid-egress and mid-ingress phases is consistent with the expected width of the white dwarf eclipse,  $\Delta\phi = 0.0662 \pm 0.0002$  cycle (Baptista et al. 1998). Finally, we adopt a cycle number representative of the ensemble of light curves and use the same test ephemeris to compute the corresponding observed mid-eclipse time (HJD) for this cycle including the measured value of  $\phi_0$ . This yields a single, but robust mid-eclipse timing estimate from a sample of eclipse light curves. For V2051 Oph these measurements have a typical accuracy of about 5 s.

Figure 1 shows the measurements of mid-eclipse timings with this procedure on average light curves of V2051 Oph at three different occasions. The sharp breaks in the slope of the light curves correspond to the ingress/egress features of the white dwarf and provide a precise determination of the mid-eclipse phase  $\phi_0$ .

The mid-eclipse timings are independent of passband.

**Table 2.** Mid-eclipse timings of V2051 Oph.

Cycle	HJD (2,400,000+)	BJDD (2,400,000+)	(O-C) <sup>a</sup> (cycles)
24	43247.47528	43247.47586 (5)	+0.0011
1 154	43318.01879	43318.01937 (5)	+0.0015
2 038	43373.20507	43373.20565 (6)	+0.0023
5 911	43614.98815	43614.98874 (6)	+0.0018
12 778	44043.68031	44043.68089 (7)	+0.0022
22 888	44674.82576	44674.82633 (6)	-0.0020
24 342	44765.59587	44765.59644 (6)	-0.0021
29 789	45105.64044	45105.64100 (9)	-0.0022
64 820	47292.55070	47292.55135 (6)	-0.0044
65 845	47356.53932	47356.53997 (5)	-0.0034
70 999	47678.29257	47678.29323 (6)	-0.0026
77 594	48090.00424	48090.00491 (6)	-0.0039
81 482	48332.72384	48332.72451 (7)	-0.0029
84 241	48504.96234	48504.96301 (6)	-0.0025
89 504	48833.52016	48833.52082 (5)	-0.0030
109 989	50112.35515	50112.35581 (4)	+0.0003
112 217	50251.44442	50251.44508 (2)	+0.0002
124 545	51021.05518	51021.05589 (2)	+0.0018
130 199	51374.02226	51374.02299 (2)	+0.0012
136 294	51754.52000	51754.52074 (4)	+0.0000
141 636	52088.00958	52088.01033 (2)	-0.0010
148 100	52491.54297	52491.54371 (6)	-0.0061

<sup>a</sup> Observed minus calculated times with respect to the linear ephemeris of Table 3.

The measured timings from the multicolour runs are the same at all wavelengths within the measurement errors.

For V2051 Oph the difference between universal time (UT) and terrestrial dynamical time (TDT) changed by 14 s over the 26 yr time span of our observations. The amplitude of the difference between the barycentric and the heliocentric corrections is about 7 s. The mid-eclipse timings have been calculated on the solar system barycentre dynamical time (BJDD), according to the code by Stumpff (1980). The terrestrial dynamical (TDT) and ephemeris (ET) time scales were assumed to form a contiguous scale for our purposes. The new eclipse timings are listed in Table 2. The corresponding uncertainties in the last digit are indicated in parenthesis.

The data points were weighted by the inverse of the squares of the uncertainties in the mid-eclipse times. Table 3 presents the parameters of the best-fit linear, quadratic and linear plus sinusoidal ephemerides with their 1- $\sigma$  formal errors quoted. We also list the root-mean-squares of the residuals,  $\sigma$ , and the  $\chi^2_{\nu_2}$  value for each case, where  $\nu_2$  is the number of degrees of freedom.

Fig. 2 presents the (O-C) diagram with respect to the linear ephemeris in Table 3. The new timings are indicated as solid circles and show a clear modulation. Open squares show the individual eclipse timings taken from the literature (Warner & Cropper 1983; Cook & Brunt 1983; Bauermann & Pakull 1984; Watts et al. 1986; Watts & Watson 1986; Warner & O'Donoghue 1987; Hollander, Kraakman & van Paradijs 1993; Echevarria & Alvares 1993; Baptista et al. 1998) and individual eclipse timings measured from our light curves using the bisected chord method. All individual timings were corrected to BJDD. The individual timings show a large scatter, of about 40 s, and are generally later than the contemporary mid-eclipse timings in Table 2. We will return to this point in section 3.

**Table 3.** Ephemerides of V2051 Oph.

<b>Linear ephemeris:</b>	
BJDD = $T_0 + P_0 \cdot E$	
$T_0 = 2\,443\,245.977\,52 (\pm 3)$ d	$P_0 = 0.062\,427\,8634 (\pm 3)$ d
$\chi^2_{\nu_2} = 9.5, \nu_2 = 20$	$\sigma_1 = 2.69 \times 10^{-3}$ cycles
<b>Quadratic ephemeris:</b>	
BJDD = $T_0 + P_0 \cdot E + c \cdot E^2$	
$T_0 = 2\,443\,245.977\,59 (\pm 3)$ d	$P_0 = 0.062\,427\,859 (\pm 1)$ d
$c = (+3.2 \pm 0.8) \times 10^{-14}$ d	$\sigma_2 = 2.29 \times 10^{-3}$ cycles
$\chi^2_{\nu_2} = 8.5, \nu_2 = 19$	
<b>Sinusoidal ephemeris:</b>	
BJDD = $T_0 + P_0 \cdot E + A \cdot \cos [2\pi(E - B)/C]$	
$T_0 = 2\,443\,245.977\,45 (\pm 4)$ d	$B = (120 \pm 6) \times 10^3$ cycles
$P_0 = 0.062\,427\,8629 (\pm 4)$ d	$C = (127 \pm 8) \times 10^3$ cycles
$A = (20 \pm 4) \times 10^{-5}$ d	$\sigma_S = 1.22 \times 10^{-3}$ cycles
$\chi^2_{\nu_2} = 2.5, \nu_2 = 17$	

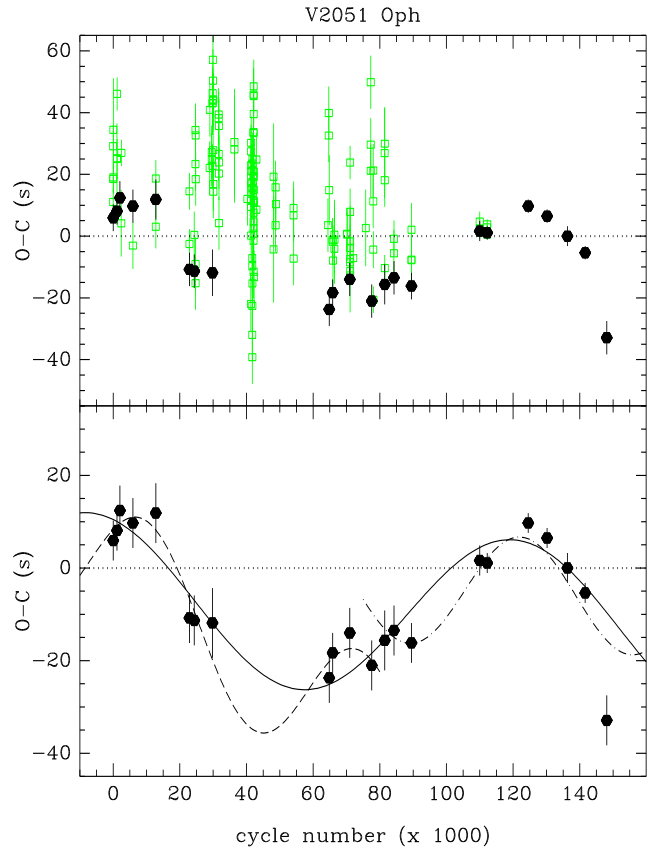


**Figure 2.** The (O-C) diagram of V2051 Oph with respect to the linear ephemeris of Table 3. The eclipse timings from the literature and individual timings measured from our light curves using the bisected chord method are shown as open squares, while the new mid-eclipse timings are indicated as solid circles. The solid line in the lower panel shows the best-fit linear plus sinusoidal ephemeris of Table 3. The dashed and dot-dashed lines in the lower panel show the best-fit 11 yr cycle period sinusoidal ephemeris, respectively, for the data in the first and the second halves of the time interval.

The significance of adding additional terms to the linear ephemeris was estimated by using the F-test, following the prescription of Pringle (1975). The quadratic ephemeris has a statistical significance of 98.6 per cent with an  $F(3, 19) = 7.2$ . On the other hand, the statistical significance of the linear plus sinusoidal ephemeris with respect to the linear fit is larger than 99.99 per cent, with an  $F(3, 17) = 65.6$ . The best-fit period of the modulation is  $22 \pm 2$  yr. The best-fit linear plus sinusoidal ephemeris is shown as a solid line in the lower panel of Fig. 2.

However, the eclipse timings show systematic and significant deviations from the best-fit linear plus sinusoidal ephemeris. The fact that  $\chi^2_{\nu_2} > 1$  emphasizes that the linear plus sinusoidal ephemeris is not a complete description of the data, perhaps signalling that the period variation is not sinusoidal or not strictly periodic.

We explored these possibilities by making separate fits to the first half of the data set ( $E < 75 \times 10^3$  cycle) and to the second half of the data set ( $E > 75 \times 10^3$  cycle). The first half of the data set can be well described by ephemerides with cycle periods of 11 and 5.5 yr. The best-fit cycle period for the second half of the data set is the same as that obtained for the whole data set under the uncertainties. This part of the data set can also be reasonably well described by ephemerides of cycle periods of 11 and 7 yr. The 7 yr period is consistent with the 6.87 yr cycle period previously found by Echevarria & Alvares (1993). We note that 11, 7 and 5.5 yr periods are, respectively, the first, second and third harmonics of the 22 yr main period modulation. The 11 yr period best-fit ephemerides for the first and second halves of the data set are shown in the lower panel of Fig. 1, respectively, as the dashed and dot-dashed curves. These results indicate that the period changes in V2051 Oph are not sinusoidal or not strictly periodic.

## 2.2 V4140 Sgr

V4140 Sgr was observed with the 1.6 m telescope at LNA from 1985 to 2000. The reader is referred to Baptista et al. (1989; 1992) for a detailed description of the data sets and of the reduction procedures for the observations prior to 1992. The new observations (1992–2000) were performed with the same CCD photometer as those of V2051 Oph except for the run of 1996 June, which was collected with the photoelectric photometer. The data reduction in each case is identical to that described in section 2.1.

The journal of the new observations is shown in Table 4. The notation is the same as in Table 1. The data comprise 57 eclipse light curves spanning 16 yr of observations. Only runs while V4140 Sgr was in quiescence were included in the analysis. The observations of the eclipse cycles 18782–18783, 18798–18801, and 30228–30229 (Baptista et al. 1992) were excluded because V4140 Sgr was in outburst at those epochs.

Mid-eclipse times of the white dwarf were measured for the ensemble of light curves of each season with the technique described in section 2.1. The accuracy of these measurements for V4140 Sgr is better than 12 s. The lower accuracy is mainly the consequence of V4140 Sgr being 3 magnitudes fainter than V2051 Oph.

For V4140 Sgr the difference between the UT and TDT scales changed by 6 s over the 16 yr span of our data set,

**Table 4.** The new observations of V4140 Sgr.

Date (UT)	Passband	$\Delta t$ (s)	Cycle
1992 Jul 29	V	15	41 867–41870
1992 Jul 30	V	15	41 882–41887
1996 Jun 16	W	15	64 955
1998 Jul 26	B	20	77 488, 77 489
1999 Jul 12	B	20	83 200, 83 202
1999 Jul 14	B	20	83 236
2000 Jul 29	B	20	89 436
2000 Jul 30	B	20	89 449, 89 451

**Table 5.** Mid-eclipse timings of V4140 Sgr.

Cycle	HJD (2,400,000+)	BJDD (2,400,000+)	(O–C) <sup>a</sup> (cycles)
12	46262.40830	46262.40889 (7)	+0.0046
5 179	46579.81529	46579.81589 (9)	+0.0023
13 080	47065.17109	47065.17172 (10)	+0.0013
17 826	47356.71619	47356.71683 (7)	–0.0008
23 162	47684.50477	47684.50543 (6)	–0.0036
30 065	48108.55396	48108.55463 (11)	–0.0013
35 580	48447.33864	48447.33931 (13)	–0.0013
41 878	48834.22291	48834.22358 (13)	+0.0014
64 955	50251.83520	50251.83585 (13)	–0.0053
77 488	51021.73363	51021.73431 (6)	–0.0004
83 213	51373.41854	51373.41923 (6)	–0.0000
89 445	51756.24831	51756.24903 (4)	+0.0006

<sup>a</sup> Observed minus calculated times with respect to the linear ephemeris of Table 6.

and the amplitude of the difference between the barycentric and the heliocentric corrections is about 4 s. The mid-eclipse timings were calculated in BJDD according to the code by Stumpff (1980) and are listed in Table 5. The corresponding uncertainties in the last digit are indicated in parenthesis.

We fitted linear, quadratic and linear plus sinusoidal ephemerides to the eclipse timings in Table 5. The data points were weighted by the inverse of the squares of the uncertainties in the mid-eclipse times. Table 6 shows the parameters of the best-fit ephemerides with their 1- $\sigma$  formal errors quoted. The values of  $\sigma$  and  $\chi^2_{\nu_2}$  for each case are also listed.

Fig. 3 shows the (O–C) diagram with respect to the linear ephemeris in Table 6. The new timings are indicated

**Table 6.** Ephemerides of V4140 Sgr.

**Linear ephemeris:**

$$\text{BJDD} = T_0 + P_0 \cdot E$$

$$T_0 = 2\,446\,261.671\,45 (\pm 6) \text{ d} \quad P_0 = 0.061\,429\,6779 (\pm 9) \text{ d}$$

$$\chi^2_{\nu_2} = 4.2, \quad \nu_2 = 10 \quad \sigma_1 = 2.62 \times 10^{-3} \text{ cycles}$$

**Quadratic ephemeris:**

$$\text{BJDD} = T_0 + P_0 \cdot E + c \cdot E^2$$

$$T_0 = 2\,446\,261.671\,68 (\pm 7) \text{ d} \quad P_0 = 0.061\,429\,660 (\pm 5) \text{ d}$$

$$c = (+1.8 \pm 0.5) \times 10^{-13} \text{ d} \quad \sigma_2 = 1.88 \times 10^{-3} \text{ cycles}$$

$$\chi^2_{\nu_2} = 1.74, \quad \nu_2 = 9$$

**Sinusoidal ephemeris:**

$$\text{BJDD} = T_0 + P_0 \cdot E + A \cdot \cos [2\pi(E - B)/C]$$

$$T_0 = 2\,446\,261.671\,50 (\pm 4) \text{ d} \quad B = (3 \pm 2) \times 10^3 \text{ cycles}$$

$$P_0 = 0.061\,429\,6757 (\pm 7) \text{ d} \quad C = (41 \pm 2) \times 10^3 \text{ cycles}$$

$$A = (19 \pm 6) \times 10^{-5} \text{ d} \quad \sigma_S = 0.92 \times 10^{-3} \text{ cycles}$$

$$\chi^2_{\nu_2} = 0.71, \quad \nu_2 = 7$$

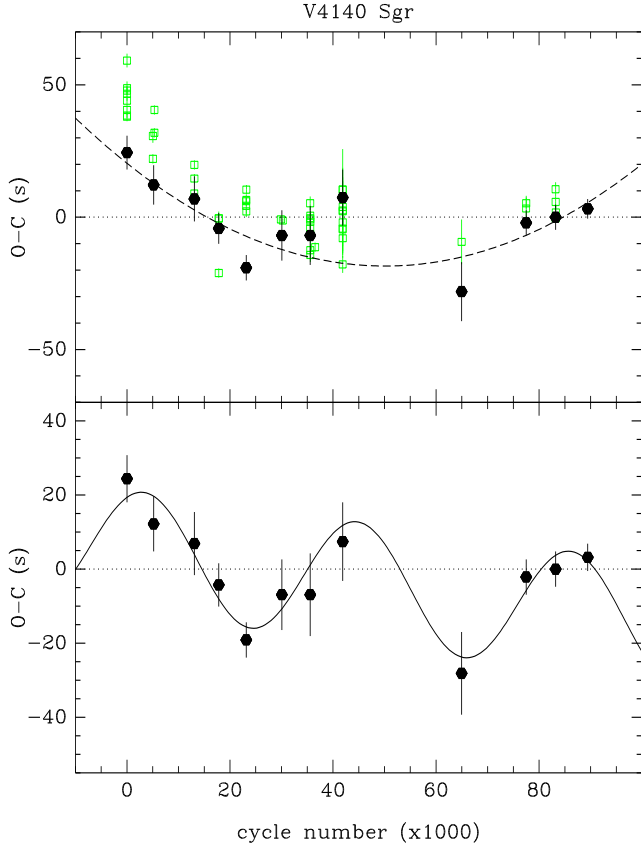


**Figure 3.** The (O–C) diagram of V4140 Sgr with respect to the linear ephemeris of Table 6. The individual timings from the literature and eclipse timings measured from our individual light curves using the bisected chord method are shown as open squares, while the new timings are indicated as solid circles. The dashed line in the upper panel depicts the best-fit quadratic ephemeris while the solid line in the lower panel shows the best-fit linear plus sinusoidal ephemeris of Table 6.

as solid circles. Open squares show the timings from the literature and individual eclipse timings measured from our new light curves using the bisected chord method. These timings were corrected to BJDD. Similar to Fig. 2, the individual timings show a tendency to be later than the white dwarf mid-eclipse timing of the ensemble. This effect will be addressed in section 3.

From the  $\sigma_1$  and  $\sigma_2$  values in Table 6 we obtain  $F(3, 9) = 8.5$ , which corresponds to a 98.3 per cent confidence level for the quadratic ephemeris. This is less than the 99.7 per cent confidence level previously found by Baptista et al. (1992). The quadratic term is a factor of 2.4 times smaller than that derived by those authors. The best-fit quadratic ephemeris is depicted as a dashed line in the upper panel of Fig. 3. The linear plus sinusoidal ephemeris is statistically significant at the 99.97 per cent level for an  $F(3, 7) = 49.8$ . The dispersion of the data with respect to the fit is reduced by a factor of 2 in comparison with the quadratic ephemeris. The best-fit period of the modulation in V4140 Sgr is  $6.9 \pm 0.3$  yr. The best-fit linear plus sinusoidal ephemeris is shown as a solid line in the lower panel of Fig. 3. A search for a variable cycle period or for harmonics of the main cycle period (by performing separate fits to different

parts of the data set) is not conclusive in this case because of the relatively small number of mid-eclipse timings.

### 3 DISCUSSION

#### 3.1 On the large dispersion of the V2051 Oph eclipse timings

V2051 Oph shows large amplitude flickering which distorts its eclipse shape (e.g., Warner & Cropper 1983) and affects the measurement of eclipse times. The large dispersion in the individual eclipse timings in comparison with our results can be partly attributed to the highly variable shape of the eclipse in V2051 Oph and partly to the variety of methods employed by different authors to measure their eclipse timings. Some of the authors measure times of minimum light (e.g., Hollander et al. 1993), while others quote the time corresponding to the centroid of the eclipse<sup>‡</sup> (e.g., Warner & O’Donoghue 1987). None of the individual timings in the literature correspond to the mid-eclipse of the white dwarf. This is not surprising since the white dwarf eclipse features are not easy to see in individual light curves because of flickering.

Eclipses of cataclysmic variables are usually asymmetric because of the non-negligible contribution of the bright spot to the total light. In the case of quiescent dwarf novae – where the accretion disc is relatively faint in comparison to the white dwarf and the bright spot – the asymmetry is even more pronounced, leading to a double-stepped eclipse shape (p.ex., Fig. 1).

For such asymmetric eclipse shape, both the times of minimum light and of the centroid of the eclipse will be affected by the relative brightness and by the position of the bright spot with respect to the line joining the stars. Times of minimum light tend to be later than the times of the centroid of the eclipse. Both of them are later than the white dwarf mid-eclipse time. The difference between these three quantities increase with the relative brightness of the bright spot.

By combining many eclipse light curves we are able of reducing the influence of flickering in the determination of the eclipse timing. By applying a unique measurement procedure to all data set and by adopting the white dwarf mid-eclipse as our timing reference we are able of minimizing the internal inconsistencies affecting the individual timings in the literature.

The lesson Fig. 2 tells us is that the ability to identify small amplitude ( $\lesssim 40$  s) orbital period modulations may be considerably limited with (O–C) diagrams based on individual eclipse timings measured with different methods.

#### 3.2 Upper limits for secular period changes

The statistical significance of the quadratic ephemerides of V2051 Oph and V4140 Sgr is below the  $3\text{-}\sigma$  level and is highly dependent on the eclipses timings included in the

<sup>‡</sup> usually referred in the literature as the mid-eclipse time.

fit. For example, if the first timing of V4140 Sgr is not included in the fit the significance of the resulting quadratic ephemeris drops to 93 per cent.

This behaviour is easy to understand if we assume that the period cyclical modulation is real. In the limit where the observing baseline covers a small number of cycles of the period modulation, the sign and the magnitude of the quadratic term are affected by the number of maxima and minima comprised by the baseline. In the case of equal number of maxima and minima, the quadratic term of a parabolic fit will tend to zero (or, to the true quadratic trend in the data set). If there are more maxima (minima) than minima (maxima), the quadratic term will tend to be positive (negative). For V2051 Oph, the observations cover two maxima and one minimum of the modulation and the quadratic term of the parabolic fit is positive. For V4140 Sgr there are three maxima and two minima in the baseline, also leading to a positive quadratic term. Hence, we conclude that there is not yet evidence of secular period increase/decrease in these two binaries.

We may use the computed quadratic term to derive a  $3\sigma$  upper limit to a secular period change. For V2051 Oph this gives  $|\dot{P}| < 3 \times 10^{-12}$ , corresponding to a timescale for secular period change of  $\tau_P > 5.6 \times 10^7$  yr. These numbers are a factor of about 5 times more restrictive than those previously derived by Echevarria & Alvares (1993). For V4140 Sgr we find  $|\dot{P}| < 1.8 \times 10^{-11}$  and  $\tau_P > 9.6 \times 10^6$  yr.

An upper limit to the mass transfer rate in the binary can be obtained from the timescale  $\tau_P$ . Using a power law to express the response of the radius of the secondary star to mass loss,  $R_2(t) \propto [M_2(t)]^\beta$ , the mass transfer rate  $\dot{M}_2$  can be written in terms of  $\tau_P$  as (Molnar 1988; Robinson et al. 1991),

$$\frac{\dot{M}_2}{M_2} = \left( \frac{2}{3\beta - 1} \right) \frac{1}{\tau_P} = \frac{1.6}{\tau_P}, \quad (1)$$

where we assumed  $\beta = 0.75$  (Smith & Dhillon 1998). Adopting  $M_2 = 0.15 M_\odot$  (Baptista et al. 1998) and  $M_2 = 0.09 M_\odot$  (Borges & Baptista 2003, private communication), we find  $\dot{M}_2 < 4.3 \times 10^{-9} M_\odot \text{ yr}^{-1}$  and  $\dot{M}_2 < 1.5 \times 10^{-8} M_\odot \text{ yr}^{-1}$ , respectively, for V2051 Oph and V4140 Sgr.

### 3.3 Cyclical period changes

Our results reveal that the orbital period of V2051 Oph shows conspicuous cyclical, quasi-periodic changes of amplitude 17 s on a time-scale of about 22 yr. V4140 Sgr shows a similar period modulation on a time-scale of 6.9 yr.

Cyclical orbital period changes are seen in many eclipsing CVs (Warner 1995 and references therein). The cycle periods range from 4 yr in EX Dra (Baptista et al. 2000) to about 30 yr in UX UMa (Rubenstein, Patterson & Africano 1991), whereas the amplitudes are in the range  $10^1 - 10^2$  s. Therefore, V2051 Oph and V4140 Sgr fit nicely in the overall picture drawn from the observations of orbital period changes in CVs.

If one is to seek for a common explanation for the cyclical period changes in CVs, then models involving apsidal motion or a third body in the system shall be discarded as these require that the orbital period change be strictly periodic, whereas the observations show that this is not the case

(Richman et al. 1994 and references therein). We may also discard explanations involving angular momentum exchange in the binary, as cyclical exchange of rotational and orbital angular momentum (Smak 1972; Biermann & Hall 1973) requires discs with masses far greater than those deduced by direct observations, and the time-scales required to allow the spin-orbit coupling of a secondary of variable radius are much shorter than the tidal synchronization scales for these systems ( $\sim 10^4$  yr, see Applegate & Patterson 1987).

The best current explanation for the observed cyclical period modulation is that it is the result of a solar-type magnetic activity cycle in the secondary star (see Applegate 1992 and references therein). Richman et al. (1994) proposed a model in which the Roche lobe radius of the secondary star  $R_{L2}$  varies in response to changes in the distribution of angular momentum inside this star (caused by the magnetic activity cycle), leading to a change in the orbital separation and, therefore, in the orbital period. As a consequence of the change in the Roche lobe radius, the mass transfer rate  $\dot{M}_2$  also changes. In this model, the orbital period is the shortest when the secondary star is the most oblate (i.e., its outer layers rotate faster), and is the longest when the outer layers of the secondary star are rotating the slowest.

The fractional period change  $\Delta P/P$  is related to the amplitude  $\Delta(O - C)$  and to the period  $P_{mod}$  of the modulation by (Applegate 1992),

$$\frac{\Delta P}{P} = 2\pi \frac{\Delta(O - C)}{P_{mod}} = 2\pi \frac{A}{C}. \quad (2)$$

Using the values of  $A$  and  $C$  in Tables 3 and 6, we find  $\Delta P/P = 1.6 \times 10^{-7}$  and  $\Delta P/P = 4.7 \times 10^{-7}$ , respectively, for V2051 Oph and V4140 Sgr.

The predicted changes in Roche lobe radius and mass transfer rate are related to the fractional period change by (Richman et al. 1994),

$$\frac{\Delta R_{L2}}{R_{L2}} = 39 \left( \frac{1+q}{q} \right)^{2/3} \left( \frac{\Delta\Omega}{10^{-3}\Omega} \right)^{-1} \frac{\Delta P}{P}, \quad (3)$$

and by,

$$\frac{\Delta \dot{M}_2}{\dot{M}_2} = 1.22 \times 10^5 \left( \frac{1+q}{q} \right)^{2/3} \left( \frac{\Delta\Omega}{10^{-3}\Omega} \right)^{-1} \frac{\Delta P}{P}, \quad (4)$$

where  $\Delta\Omega/\Omega$  is the fractional change in the rotation rate of the outer shell of the secondary star involved in the cyclical exchange of angular momentum,  $q (= M_2/M_1)$  is the binary mass ratio, and the minus signs were dropped.

Baptista et al. (2002) showed that the induced changes in mass transfer rate lead to a modulation in the quiescent brightness of a dwarf nova of  $\Delta m \simeq 0.3$  ( $\Delta \dot{M}_2/\dot{M}_2$ ). They inferred a value of  $\Delta\Omega/\Omega \simeq 2.7 \times 10^{-3}$  for Z Cha by equating the predicted change in brightness to the observed brightness modulation (Ak, Ozkan & Mattei 2001). Adopting  $q = 0.19$  for V2051 Oph (Baptista et al. 1998) and  $q = 0.125$  for V4140 Sgr (Borges & Baptista 2003, priv. commun.), and assuming  $\Delta\Omega/\Omega \simeq 3 \times 10^{-3}$ , we obtain  $\Delta R_{L2}/R_{L2} \simeq 7 \times 10^{-6}$  and  $\Delta R_{L2}/R_{L2} \simeq 2.6 \times 10^{-5}$ , respectively for V2051 Oph and V4140 Sgr. This is comparable to the value obtained for Z Cha. (We found an error in the fractional change of the radius of the secondary Roche lobe of Z Cha as quoted by Baptista et al. (2002). The correct value is  $\Delta R_{L2}/R_{L2} = 2.2 \times 10^{-5}$ .)

### 3.4 The amplitude versus $P_{mod}$ diagram

The present work doubles the sample of measured  $\Delta P/P$  values for short-period eclipsing CVs and allows a qualitative comparison of cyclical period changes between systems above and below the period gap.

Figure 4 shows a diagram of the amplitude versus period of the modulation for 11 eclipsing CVs, comprising 7 long-period ( $P_{orb} > 3$  hr) and 4 short-period ( $P_{orb} < 3$  hr) systems. The absence of a few well-known eclipsing CVs in this diagram (e.g., HT Cas and OY Car) is worth a comment. The lack of evidence of cyclical period changes in these systems may be caused by selection effects, p.ex., (O–C) diagrams covering a not long enough baseline ( $\lesssim 10$  yr) or with a poor sampling of eclipse timings. Additionally, small amplitude period modulations may be buried in the scatter of a sample of individual eclipse timings measured with different procedures (section 3.1).

Under the framework of the magnetic activity cycle explanation, Fig. 4 allows a few interesting conclusions to be drawn. First, magnetic activity cycles seems a widespread phenomenon in the secondary stars of CVs, being equally common among long- and short-period systems. Noteworthy, even the fully convective secondary stars of the short-period CVs show magnetic activity cycles. The cycle periods are in the range from 4 to 30 yr, independent of binary orbital period.

These results are consistent with those of Ak, Ozkan & Mattei (2001). They found cyclical variations in the quiescent magnitude and outburst interval of a sample of CVs, which they attributed to solar-type magnetic activity cycles in the secondary stars. They also found no correlation of the cycle period with the rotation regime of the secondary star (i.e., orbital period, for the phase-locked secondary stars in CVs).

Thus, we collected independent evidence that the magnetic field (and activity) of the secondary stars of CVs do not disappear when they become fully convective.

Last but not least, the fractional cycle period changes of the short-period CVs [ $\Delta P/P \simeq (2 - 5) \times 10^{-7}$ ] are systematically smaller than those of the long-period CVs [ $\Delta P/P \simeq (1 - 2) \times 10^{-6}$ ]. Assuming that  $(\Delta\Omega/\Omega)$  is the same for long- and short-period systems, this leads to systematically larger fractional changes in the Roche lobe of the secondary star for the long period CVs (by a factor of  $\simeq 2.5$ ). Alternatively, assuming that the resulting  $\Delta R_{L2}/R_{L2}$  are comparable for long- and short-period CVs, the above implies that the  $(\Delta\Omega/\Omega)$  values are systematically larger by a factor of  $\simeq 2.5$  for the long-period systems. This effect may be a consequence of the different internal structures of secondary stars of long- and short-period CVs or it may alternatively be a manifestation of a lower intensity magnetic field in the short-period CVs.

Investigation of period changes in CVs have usually been done by collecting individual timings in the literature and adding new ones to construct updated (O–C) diagrams. Our analysis of the V2051 Oph data shows that more elaborated procedures, such as the one described in this paper, are probably required in order to find low-amplitude cyclical period changes in short-period CVs. The extension of the sample of systems in the amplitude versus  $P_{mod}$  diagram, particularly with the addition of more short-period

CVs, will be useful to verify, and perhaps strengthen, the conclusions drawn here.

### ACKNOWLEDGMENTS

We thank an anonymous referee for useful comments and suggestions which helped to improve the presentation of our results. This work is partly based on observations made at Laboratório Nacional de Astrofísica, Brazil. RB acknowledges financial support from CNPq through grant no. 300 354/96-7. BWB acknowledges financial support from CAPES/Brazil.

### REFERENCES

- Ak T., Ozkan M. T., Mattei J. A., 2001. *A&A*, 369, 882  
 Applegate J. H., 1992. *ApJ*, 385, 621  
 Applegate J. H., Patterson J., 1987. *ApJ*, 322, L99  
 Baptista R., Catalán M.S., Horne K., Zilli D., 1998. *MNRAS*, 300, 233  
 Baptista R., Catalán M. S., Costa L., 2000. *MNRAS*, 316, 529  
 Baptista R., Horne K., Hilditch R., Mason K. O., Drew J. E., 1995. *ApJ*, 448, 395  
 Baptista R., Jablonski F. J., Steiner J. E., 1989. *MNRAS*, 241, 631  
 Baptista R., Jablonski F. J., Steiner J. E., 1992. *AJ*, 104, 1557  
 Baptista R., Jablonski F. J., Oliveira E., Vrielmann S., Woudt P., Catalán M. S., 2002. *MNRAS*, 335, L75  
 Beuermann K., Pakull M. W., 1984. *A&A*, 136, 250  
 Biermann P. L., Hall D., 1973. *A&A*, 27, 249  
 Bond H. E., 1977. *IAU Circ.* 3065  
 Bond I. A., Freeth R. V., 1988. *MNRAS*, 232, 753  
 Cook M. C., Brunt C. C., 1983. *MNRAS*, 205, 465  
 Echevarria J., Alvarez M., 1993. *A&A*, 275, 187  
 Graham J. A., 1982. *PASP*, 94, 244  
 Grauer A. D., Bond H. E., 1981. *PASP*, 93, 388  
 Hameury J. M., King A. R., Lasota J. P., 1991. *A&A*, 248, 525  
 Hollander A., Kraakman H., van Paradijs J., 1993. *A&AS*, 101, 87  
 King A. R., 1988. *QJRAS*, 29, 1  
 Lamla E., 1981. *Landolt-Börnstein - Numerical Data and Functional Relationships in Science and Technology*, Vol. 2, eds. K. Schaifers & H. H. Voigt, Springer-Verlag  
 Landolt A. U., 1983. *AJ*, 88, 439  
 Molnar L. A., 1988. *ApJ*, 331, L25  
 Pringle J., 1975. *MNRAS*, 170, 633  
 Richman H. R., Applegate J. H., Patterson J., 1994. *PASP*, 106, 1075  
 Robinson E. L., Shetrone M. D., Africano J. L., 1991. *AJ*, 102  
 Rubenstein E. P., Patterson J., Africano J. L., 1991. *PASP*, 103, 1258  
 Smak J. I., 1972. *Acta Astr.*, 22, 1  
 Smith D. A., Dhillon V. S., 1998. *MNRAS*, 301, 767  
 Stone R. P. S., Baldwin J. A., 1983. *MNRAS*, 204, 347  
 Stumpff P., 1980. *A&AS*, 41, 1  
 Warner B., 1988. *Nature*, 336, 129  
 Warner B., 1995. *Cataclysmic Variable Stars*, Cambridge University Press, Cambridge  
 Warner B., Cropper M., 1983. *MNRAS*, 203, 909  
 Warner B., O'Donoghue D., 1987. *MNRAS*, 224, 733  
 Watts D. J., Bailey J., Hill P. W., Greenhill J. G., McCowage C., Carty T., 1986. *A&A*, 154, 197  
 Watts D. J., Watson R. D., 1986. *Proc. ASA*, 6, 306  
 Wolf S., Mantel K. H., Horne K., Barwig H., Schoembs R., Baernbantner O., 1993. *A&A*, 273, 160



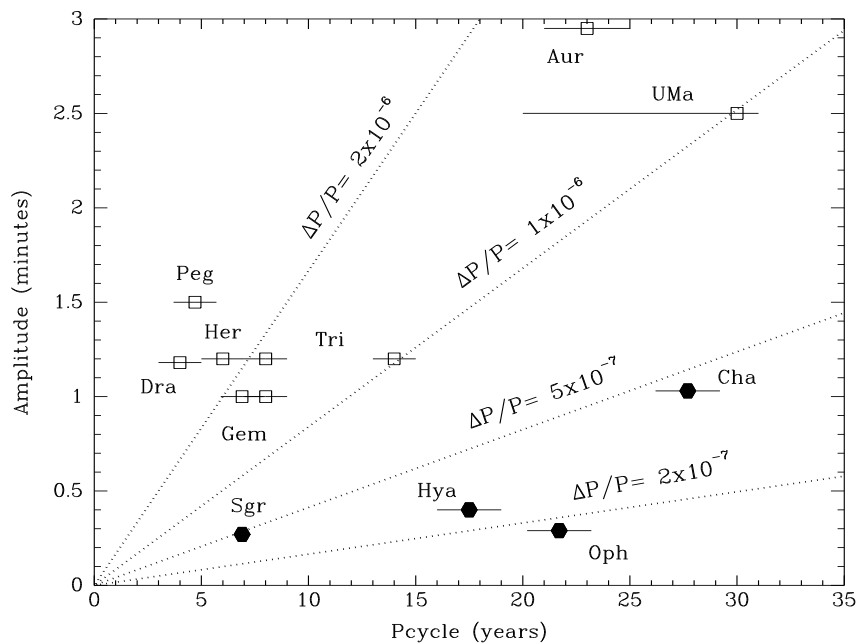


**Figure 4.** Diagram of the amplitude versus period of the modulation for eclipsing CVs. Lines of constant fractional period change  $\Delta P/P$  are shown as dotted lines. Long period systems ( $P_{orb} > 3$  hr) are shown as open squares, short period system ( $P_{orb} < 3$  hr) are indicated by filled circles. The diagram include measurements of the following stars: V2051 Oph, V4140 Sgr (this paper), Z Cha (Baptista et al. 2002), EX Dra (Baptista, Catalán & Costa 2000), and EX Hya, U Gem, IP Peg, DQ Her, RW Tri, T Aur and UX UMa (Warner 1995 and references therein).

Wood J. H., Irwin M. J., Pringle J. E., 1985. MNRAS, 214, 475

This paper has been produced using the Royal Astronomical Society/Blackwell Science L<sup>A</sup>T<sub>E</sub>X style file.